OpenNano 7 (2022) 100060

Contents lists available at ScienceDirect

OpenNano

journal homepage: www.elsevier.com/locate/onano

Review article

The effectiveness of silver nanoparticles as a clean-up material for water polluted with bacteria DNA conveying antibiotics resistance genes: Effect of different molar concentrations and competing ions

Adaora S. Ezeuko [a,c,*], Mike O. Ojemaye [a,c], Omobola O. Okoh [a,c], Anthony I. Okoh [b,c]

[a] Department of Pure and Applied Chemistry, University of Fort Hare, Alice 5700, South Africa
[b] Department of Environmental Health Sciences, College of Health Sciences, University of Sharjah, United Arab Emirates
[c] SAMRC, Microbial Water Quality Monitoring Centre, University of Fort Hare, Alice, South Africa

ARTICLE INFO

Keywords:
Silver nanoparticles
Adsorption
Antibiotic resistance genes
DNA
Equilibrium study

ABSTRACT

This study employed silver nanoparticles to remove DNA conveying antibiotic resistance genes from water. Three different molar concentrations of silver nanoparticles represented as BD1 (0.1 M), BD2 (0.5 M), and BD3 (1.0 M) were synthesized as adsorbents and evaluated in a batch adsorption system for the removal of bacteria DNA conveying antibiotic resistance genes from simulated aqueous solution. The authenticity of the adsorbents was confirmed by characterization techniques using Fourier transformed infrared spectroscopy (FTIR), scanning electron microscopy (SEM) coupled with energy-dispersive x-ray spectroscopy (EDX), and x-ray diffraction spectroscopy (XRD) indicated the successful synthesis of these AgNPs. Adsorption studies involving the different operating conditions on the synthesized materials showed that pH affects the removal of DNA with increased removal efficiency observed at acidic pH (removal percentage ranging from 50.26-87.61%, 65.80-87.79%, and 69.23-87.92% for BD1, BD2, and BD3 respectively). Maximum adsorption equilibrium was achieved after 180, 195, and 225 mins for BD1, BD2, and BD3. The isotherm study revealed that Langmuir model is the best fit compared to Freundlich model with highest correlation coefficient and reduced Chi-square (X^2) of $R^2 = 0.97625$ and $X^2 = 0.12142$, $R^2 = 0.96049$ and $X^2 = 0.24403$, $R^2 = 0.85108$ and reduced $X^2 = 1.00914$ for BD1, BD2, and BD3 respectively. The kinetic study for the adsorption process indicates that the adsorption of bacteria DNA onto AgNPs obeyed pseudo-second-order with the highest R^2 values (ranging from 0.90 to 0.98). Similarly, competing ions (cations and anions) influenced the adsorption capacity in this study. Therefore, this study concludes that AgNPs demonstrated effectiveness in removing bacteria DNA-conveying ARGs from water and will serve as an excellent option to tackle the menace of ARGs in water.

1.0. Introduction

The interference of antibiotic resistome in wastewater treatment facilities (WWTFs) has become a global challenge of increasing environmental concern. It poses a considerable health risk to the public due to the release of untreated effluent from the hospital,

* Corresponding author.
E-mail addresses: 201927090@ufh.ac.za, adajesusd4@gmail.com (A.S. Ezeuko).

https://doi.org/10.1016/j.onano.2022.100060
Received 20 April 2022; Received in revised form 5 July 2022; Accepted 12 July 2022
Available online 15 July 2022

domestic, agricultural, and pharmaceutical industries into WWTFs [76]. Research cleaning up bacteria DNA contaminants from WWTFs has recently interested environmental researchers and wastewater treatment management. Bacteria is responsible for about 91% of food-borne diseases, clinically treated with antibiotics [73]. The residues may be directly or indirectly discharged into WWTFs and other water matrices such as feces and urine from households and hospitals. Another way of transferring bacteria into WWTFs is the discharge of untreated effluents from agricultural farms and pharmaceutical industries into the water source. Consumption of bacteria-contaminated water causes diarrhea, vomiting, headaches, fever, fatigue, cramps, nausea, etc. These illnesses increase morbidity and mortality rate among humans and animals. The bacteria acquire antibiotic resistance when exposed to different antibiotics during treatment. Antibiotic resistance (A.R.) is carried by antibiotic-resistant bacteria (ARB) and conveyed as antibiotics resistance genes (ARGs) [14,83]. The bacteria acquire ARGs in their deoxyribonucleic acid (DNA) through promiscuous gene transfers such as a conjugative plasmid, transposable elements, and integron, including genes encoding antibiotic resistance from one bacterium to another [13]. ARB transfers ARGs vertically from one bacterium to another in the water environment, making ARGs exist permanently. In addition, ARGs disseminate in the water environment via horizontal gene transfer (HGT), with mobile genetic elements which transfer ARGs through conjugation, transduction, and transformation medium [16]. HGT is the most effective medium for spreading ARGs from ARB to water environmental bacteria [2,11]. It transfers genetic material from one bacterium to another bacteria of the same and different species [20,72].

Bacteria DNA conveying ARGs have been reported to exist in the influent and effluent of WWTFs and natural waters. Excessive application of antibiotics promotes the accumulation of antibiotic-resistant bacteria (ARB) and antibiotics resistance genes (ARGs). Over 90% of antibiotics residues are discharged directly into WWTFs or other water matrices [42,59]. The exposure of these bacteria to different antibiotics synergistically promotes resistance mechanisms [67,77]. Therefore, adequate clean-up strategies are vital in preventing ARG diffusion in WWTFs and other water environments.

DNA is a molecule made up of nucleotides. Each nucleotide comprises components: a phosphate group (phosphorous atom bonded to an oxygen atom), a sugar group, and a nitrogenous base [2,31]. It is a nucleic acid containing genetic instructions for all cellular life development and proper functioning. Untreated effluents from hospital, domestic and pharmaceutical industries are the carrier of bacteria DNA conveying ARGs because these sources extensively use large quantities of antibiotics [25,90]; it is feasible that ARGs originate from these sources. Their casualties are on the rise due to the design of WWTFs and the lack of treatment material that would halt the widespread of this toxic contaminant (ARGs).

WWTFs are the facilities that allow the combination of treatment methods such as physical, chemical, and biological processes to purify or remove contaminants from wastewater [22,32]. WWTFs have been known as a "hotspot" for bacteria DNA conveying ARGs, especially those receiving effluents from hospital and pharmaceutical industries [39,61,63]. The effluents from these sources affect the water treatment process because the design of WWTFs cannot effectively eradicate pharmaceutical products. WWTFs across the globe have been reported to have high nutrient content, large microbial density, and subinhibitory concentration of antibiotics [10,48]. These features make it a comfortable environment for disseminating bacteria DNA conveying ARGs. A survey carried out between 2015 to 2020 on ARG incidence across six continents (Africa, Asia, Australia, Europe, North America, and South America) confirmed the occurrence of high ARG concentrations [25]. Still, few studies have proposed methods of eradicating these toxic contaminants from WWTFs. However, this concern has led to finding efficient and adequate treatment materials and methods to eradicate bacteria DNA conveying ARGs from WWTFs effectively. Several treatment methods and materials could remove a large amount of antibiotic residue and ARB from wastewater, but they are ineffective in removing ARGs [21,27]. Conventional, advanced oxidation processes and biodegradation treatment materials and methods effectively eradicate a substantial amount of antibiotics and ARB but are ineffective in removing ARGs [30,93].

Nanomaterials' adsorption treatment strategies could be one of the best physical treatment strategies for removing ARGs due to the high specific surface area possessed by the adsorbents [4,68]. The adsorption process design allows other intense wastewater treatment strategies to ensure more effective removal of contaminants from wastewater. Moreover is cost-effective, efficient, and the best physical method for removing antibiotics-related contaminants and other pharmaceuticals from wastewater [71]. Their unique features, such as size-dependent properties, large surface area, high degree of functionalization, and affinity to bind positive or negative contaminants, are responsible for their excellent removal of toxic contaminants from wastewater [19,85]. Also, they are known to contain a high capacity for contaminants removal and are very easy to recover after treatment. Several nanomaterials such as titanium [43], graphene oxides [12], silica [51], and cerium oxide (Anthony et al., 2020) have been employed to remove ARGs from wastewater. Among all, silver nanoparticles (AgNPs) seem to have unique potential for the inactivation of bacteria DNA and removal from wastewater through electrostatic interaction [25,70].

AgNPs are a material that is widely used for surface coating, reducing bacterial infection in food, dermal formulations, and water [65]. AgNPs are synthesized through ultrasound irradiation, chemical reduction, microwave dielectric heating, and electrochemical and green methods [46]. AgNPs possess unique properties such as optical, electrical, catalytic, and binding properties [7]. It can inhibit DNA replication through oxidative stress and prevent bacteria from producing resistance [75]. The particle size, morphology, structure, and size distribution can be controlled by the synthesis concentration of the precursor [37]. The large surface area of AgNPs increases high surface energy, which promotes surface reactivity and sorption in the adsorptive site. AgNPs formed particle size in the range of 1-100nm with an oxidation state of 0, +1, +2, and +3, which have an affinity to target negative contaminants in an aqueous solution [79]. AgNPs are easy to synthesize, cost-effective, eco-friendly, and exhibit strong antibacterial properties that could stop the proliferation of bacteria [63]. Due to these excellent properties and the fact that bacteria DNA are highly negative in their backbone [26], The authors hypothesized that removing bacteria DNA conveying ARGs could be significantly achieved using AgNPs (positively charged nanoparticles) as adsorbent. Therefore, we investigated the efficiency of different molar concentrations (0.1M, 0.5 M, and 1.0 M) of silver nanoparticles (AgNPs) as adsorbents to remove DNA conveying ARGs from water. The kinetics and isotherm parameters for

the adsorption process were also investigated. This study will be the first to report on removing DNA conveying ARGs from water using AgNPs.

2.0. Materials and methods

2.1. Chemicals

Silver nitrate ($AgNO_3$), tri-sodium citrate ($Na_3C_6H_5O_7.2H_2O$), glucose ($C_6H_{12}O_6$), and sodium hydroxides (NaOH) were purchased from Sigma Aldrich. Nuclease-free water and DNA kit were purchased from Thermo Fischer. All the chemicals used in this study were of analytical grade and used as purchased.

2.2. Synthesis and characterization of different molar concentrations of (AgNPs)

The synthesis of silver nanoparticles (AgNPs) was performed through the chemical reduction method described by [88] with slight modifications. The molar concentration of silver nitrate ($AgNO_3$) was varied to obtain different concentrations of AgNPs in ascending order of 0.1 M, 0.5 M, and 1.0 M. In contrast, the other precursors such as tri-sodium nitrate ($Na_3C_6H_5O_7.2H_2O$), glucose ($C_6H_{12}O_6$), and sodium hydroxide (NaOH) remain constant. The synthesis was performed in the following consequence. Solution A was prepared by dissolving 100 mM of $AgNO_3$ into 20 mL of distilled water. Solution B contains an equal concentration (20 Mm) of tri-sodium nitrate ($Na_3C_6H_5O_7.2H_2O$), glucose ($C_6H_{12}O_6$), and sodium hydroxide (NaOH) dissolved in 60 mL of distilled water. NaOH was added to speed up the rate of reaction. Then, solution B was allowed to heat up to 60 °C under vigorous stirring for 2 h. Solution A ($AgNO_3$) was added drop by drop and heated for 6 h at 65 °C, and stirring continued for 24 hrs. The reaction was performed in the dark. The nanoparticles were then separated by centrifugation at 4,400 rpm for 15 mins and washed several times to obtain pure AgNPs labeled BD1 (0.1 M), BD2 (0.5 M), and BD3 (1.0 M). The morphologies, functional group identification, and elemental compositions of AgNPs were determined using a scanning electron microscope (SEM) coupled with an energy dispersive x-ray spectroscope (EDX) (JOEL JSM-6390LVSEM) and Fourier transform infrared spectroscope (FTIR) (Perkin-Elmer Universal ATR 100) respectively. Ultraviolet-Visible Spectroscopy (UV-VIS) was used to analyze the concentration of synthesized samples. X-ray diffraction (XRD) (Bruker D8) determined the samples' crystallinity and phase compositions.

Table 1

2.3. Extraction and molecular characterization of bacterial DNA

The antibiotic-resistant *Vibrio Parahaemolyticus* bacteria used in this study was obtained from our laboratory archives isolated from a wastewater treatment plant University of Fort Hare, Alice. The bacteria isolate was subjected to an antibiotic susceptible test before the commencement of genomic DNA extraction. The test showed that *Vibrio Parahaemolyticus* bacteria were resistant to five (5) different antibiotic drugs. These are tetracycline, PB 300, meropenem, amikacin, and ciprofloxacin. Genomic DNA extraction was conducted using the boiling method [28] with slight modification. 12.5 g of Luria Bertani (L.B.) broth was dissolved in 500 mL of sterile distilled water and autoclaved at 121 °C for 15 mins. The solution was allowed to cool at room temperature. The bacteria

Table 1
Representation of isotherm and kinetic models, their equations, and parameters adopted in this study.

Adsorption Modeling		Equation	Parameters	Reference
Isotherm Model	**Freundlich Langmuir**	$\boldsymbol{Logqe} = logKf + \frac{1}{n} logCe$ $qe = \frac{KL\ qmCe}{1 + KLCe}$	***qe*** (μg/mL): the amount of DNA adsorbed. ***Kf*** (μg/g): Freundlich adsorption constant. ***n*** = empirical constant showing that adsorption occurred on heterogeneous surfaces through a multilayer adsorption mechanism. ***Ce***: equilibrium concentration of adsorbate. ***qe*** **(μg/g)**: the amount of DNA adsorbed per unit mass of adsorbent at equilibrium. ***qm*** **(μg/g)**: theoretical maximum adsorption capacity. $\boldsymbol{K_{L.}}$: is a Langmuir isotherm constant related to the adsorption energy **(mL/μg)**. **Ce**: equilibrium concentration	[1] [92]
Kinetic Model	**Natarajan and Khalaf First order equation**	$\log\left(\frac{Ci}{Ct}\right) = \frac{K1}{2.303\ t}$	*Ci* and *Ct* **(μg/mL)** are the initial concentration of DNA and the final amount of DNA adsorbed at contact time t (mins), respectively. $\boldsymbol{K_1}$: Adsorption rate constant for first-order equation (min^{-1})	[41]
	Pseudo-second order (PSO)	$\frac{t}{qt} = \frac{1}{K2qe2} + \frac{1}{qe}t$	$\boldsymbol{K_2}$ is the rate constant of Pseudo-second order adsorption (g/ (μg mins)). ***qe*** and ***qt*** represent the same as in the First order equation	[47]

isolates (*Vibrio Parahaemolyticus*) were suspended in the solution and incubated for 22 hours at 37 °C. After incubation, the solution was centrifuged at a speed of 5000 rpm for 10 mins, and the supernatant was decanted. The pellet obtained was suspended in 200 μL nuclease-free water, vortexed briefly, and boiled for 10 mins at 100 °C. The resulting solution was centrifuged at 13,400 rpm for 15 mins to obtain the genomic DNA. The DNA stock was stored in a -20 °C refrigerator for future analysis. The concentration and purity of DNA were measured by finding the absorbance ratio at 260 nm, 280 nm, and 320 nm using Multiparameter HACH DR 6000 Ultraviolet Spectroscopy. The polymerase chain reaction (PCRs) assay was used to confirm Vibrio Parahaemolyticus isolates, and the presence of the resistance gene was also confirmed using the primer presented in table 2. The resulting PCR products were examined using a mixture of 2% agarose gel, stained with ethidium bromide [36], pictured using the Alliance BioDoc-It System.

2.4. Batch adsorption experiment

The bacterial DNA (2 mL) was used to contaminate nuclease-free water (NFW). 20 mg of adsorbents (AgNPs) of different molar concentrations represented as BD1, BD2, and BD3 were separately weighed and added to the prepared contaminated NFW for the batch adsorption study. The effects of pH (pH range from 2 to 9 by dropwise adding 0.1 mol/L NaOH or 0.1 mol/L HCl solutions), adsorbent dosage (10-30 mg), contact time (180, 195, and 225 mins), and competing ions (0.075, 0.3, 0.093 g for cations and 0.59, 0.73 and 0.61 g for the anions) on the DNA removal from aqueous solution on each adsorbent were investigated. The experiments were conducted on a KS260 control orbital shaker at a speed of 300 rpm using 25 mL bottles with different DNA concentrations (obtained from the stock solution). After equilibration, the mixtures were subjected to centrifugal force to separate the adsorbents, and supernatants were decanted. The concentrations of DNA left in the supernatant solution were determined using a dsDNA assay kit (Q32850) Qubit 1.0 Fluorometer (Thermofischer). The amount of DNA adsorbed per unit mass (qe) of AgNPs in all the samples was calculated according to Eq. (1) and (2), respectively [29].

$$\mathrm{qe} = \frac{(Ci - Cf)}{m} \times V \tag{1}$$

$$\%\mathrm{R} = \frac{(Ci - Cf)}{Ci} \times 100 \tag{2}$$

Where qe = the adsorption capacity at equilibrium (μg/mL), V = volume of adsorbate solution (mL), m = equal to adsorbent mass (mg), C_i and C_f are the initial and final concentrations of DNA measured in μg/mL, and % R is the removal efficiency.

2.4.1. Batch kinetic studies

Kinetic experiments were performed using a similar procedure to the equilibrium experiment. The working concentrations ranging from 4.98, 9.92, and 14.98 μg/mL (obtained from DNA stock solution) were prepared, and a known adsorbents dose of 20 mg was added to each working solution. These working concentrations were decided because of the concentration of residual DNA obtained previously from municipal wastewater plants [53]. The pH 6.9 was maintained at different working concentrations. The solutions were agitated in a KS260 control orbital shaker at a speed of 300 rpm for a contact time varied from 0-to 360 minutes. The procedure was applied to all the adsorbents (BD1, BD2, and BD3) investigated at room temperature. The adsorbents from different working solutions (BD1, BD2, and BD2) were separated by centrifuging at various time intervals, and the supernatant decanted was analyzed by the same procedures as the batch adsorption experiment. The amount of residual DNA adsorbed at each time interval per unit mass of adsorbents was calculated using Eq. (1) [56]

$$\mathrm{qt} = \frac{(Ci - Ct)}{m} \times V \tag{3}$$

Where qt is adsorption capacity per time, and C_t (μg/mL) is the final DNA concentration at contact time t. All the experiments were performed in triplicate to validate the experimental data obtained. Finally, the adsorption isotherm and kinetic models were evaluated using Freundlich, Langmuir, Natarajan, and Khalaf's First order (NKFO) and Pseudo-second order (PSO) equations presented in Table 1.

2.5. Data analysis

The data obtained from this study were plotted and analyzed using OriginPro Graphing and Analysis 2021 (v.9.8.0 200), Microsoft Excel 2019, and Image J software.

Table 2
Representing the PCR primers, sequences, and protocols used in this study.

Class of Antibiotic	PCR primers	Primer sequences	Product size (bp)	PCR protocols	References
Tetracyclines	*tetA*	F: GCTACATCCTGCTTGCCTTC R: CATAGATCGCCGTGAAGAGG	210	94°C – 5 min; 35[94°C – 1 min; 55°C – 1 min; 72°C 1½ min]; 72°C – 5 min.	[82]

3.0. Results and discussion

3.1. Isolate identification and molecular characterization of bacteria DNA

The PCR product amplifications were visualized using gel electrophoresis showing the identification of *Vibrio parahaemolyticus* isolates of molecular weight of 503bp (Fig. 1a) and *tetA* resistance gene of molecular weight of 210bp (Fig. 1b). Table 2: shows the primers and PCR conditions of the targeted resistance gene.

3.2. Characterization of adsorbents

3.2.1. Point of zero charges of as-synthesized AgNPs samples (BD1, BD2, and BD3)

The Point of zero charges (PZC) of all the AgNPs samples (BD1, BD2, and BD3) was investigated. Meanwhile, the PZC is generally described as the pH at which the net charge of the total particle surface is equal to zero or neutral [89]. Fig. 2 shows that the PZC result on all the as-synthesized samples of AgNPs is in the range of 8.6, and it is similar to an already published report on the synthesis of silver nanoparticles [17]. It implies that, below this value (pH < 8.6), the surface of adsorbents acquires a positive surface charge due to protonation from the nitrate group and dissociation of $H^{+\cdot}$ [33]. Beyond 8.6 (pH > 8.6), it tends toward negative due to deprotonation of the nitrate group [44,52].

3.2.2. SEM analysis

The Scanning Electron Microscopy (SEM) analysis of as-synthesized AgNPs (BD1, BD2, and BD3) was captured at different magnifications as presented in Fig.s 3 A-B, C-D, E-F, respectively. The spherical and irregular multi-branched particles' morphology signified the particles' authenticity. The SEM micrograph revealed that adsorbents formed aggregation into clusters and bunches [8, 87]. The presence of large and small spherical particles was present, resulting in the aggregation of the particles through weak force [54].

3.2.3. EDX analysis

Energy-dispersive X-ray spectroscopy (EDX) determined the elemental composition of synthesized AgNPs represented as BD1, BD2, and BD3. Fig.s 4A (BD1), B (BD2), and C (BD3) showed the strongest signal from the Ag region and the weak signals from carbon (C) and oxygen (O). Observing optical peaks for Ag in BD1, BD2, and BD3 were observed approximately at 3 KeV, showing weight percentages (%) of 87.98, 89.65, and 90.50 and atomic percentages (%) of 47.89, 50.54, and 54.86. The result is similar to previously reported studies [35,69]. The absence of other elements confirmed the pure crystalline nature of AgNPs.

3.2.4. UV Visible Spectroscopy

Ultraviolet-visible spectroscopy (UV-Vis) is an essential and reliable technique for the characterization of synthesized metallic nanoparticles. UV-Vis was used to determine the maximum absorption of all the as-synthesized AgNPs UV-Vis spectral (Fig. 5) showed an intense absorption peak around 420 nm and 550 nm at 0.6, 0.55, and 0.49 h of incubation for BD1, BD2, and BD3. The peaks confirmed the formation of the homogenous spherical and irregular shapes of AgNPs. The result of the present study corroborates with the report obtained from the synthesis of AgNPs from Aspergillus [49]. The report has shown that homogenous AgNPs can be produced at the surface of the plasmon resonance band at 420 nm. The position and shape of the plasmon absorption band at 420 nm that led to the formation of homogenous spherical silver nanoparticles depends on the particle size, shape, and dielectric constant [34].

3.2.5. XRD analysis

X-ray diffraction (XRD) is an analytical instrument used to determine or measure a synthesized material's degree of crystalline

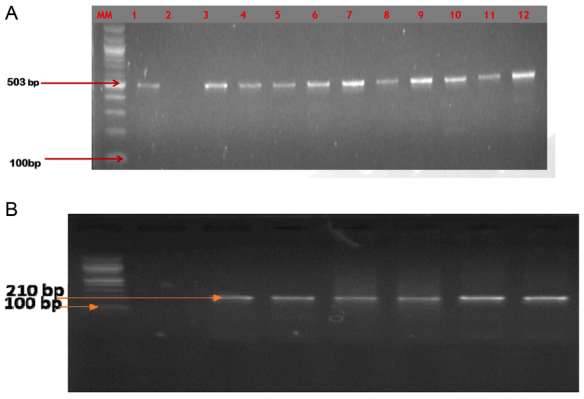

Fig. 1. (a) Gel electrophoresis of confirming *Vibrio parahaemolyticus* isolates using *toxR* gene; LMM: base pair gene marker; Lane 1: positive control; Lane 2: negative control; Lane 3-12: positive isolate. (b). Gel representing tetracycline resistance gene (*tet*A) amplified at 210 bp.

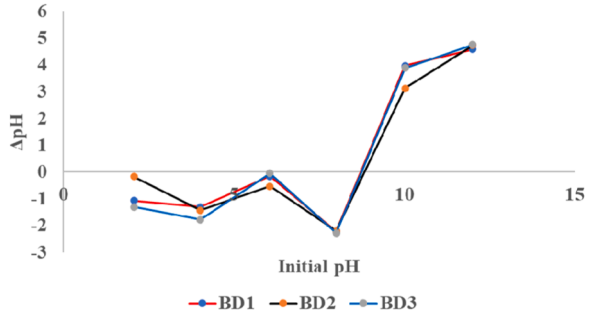

Fig. 2. PZC for the molar concentrations (0.1, 0.5 and 1.0 M) of as-synthesized AgNPs represented as BD1, BD2 and BD3.

structures, size, and phase. Fig. 6 showed the XRD pattern of the molar concentrations of as-synthesized AgNPs (BD1, BD2, and BD3) with intense diffraction peaks of 38.07° {111}, 44.87° {200}, 67.75° {220} and 77.49° {311} which corresponds to JCPDS files number 00-004-0783 [3]. The average crystallinity size of all the adsorbents was determined using the Scherrer equation [58]:

$$D = \frac{K\lambda}{\beta cos\theta} \tag{4}$$

Where D = Average crystallite size (nm)
K = Scherrer constant of 0.94 for spherical crystallites with cubic symmetry
λ = X-ray wavelength, CuKα = 1.5406 Å
β = line broadening at FWHM in radians
θ = Bragg's angle in degree, half of 2θ
The average crystalline size of all the adsorbents is BD1=BD2=BD3= 30.27 nm. The appearance of significant intense peaks confirmed the pure crystalline nature of AgNPs.

3.2.6. *FTIR spectroscopy*

FTIR spectroscopy is a non-invasive technique used to confirm vibrational bands of the active functional group present in the material. [94]. FTIR measurement (Fig. 7) revealed the potential functional group in this study's as-synthesized three adsorbents (BD1, BD2, and BD3). The FTIR profile exhibited nine (9) peaks having the following wavenumber 3320, 1622, 1550, 1450, 1388, 1296, 1071, 841, and 606 cm ^{1}. The absorbance band located at 3320 cm $^{-1}$ is assigned to the stretching vibration of N-H of primary amine. The primary amine, i.e., stretching vibration of N-H, was reported at 3413 cm^{-1} [17]. The absorbance band at 1622 cm^{-1} corresponds to $^{-}$O.H. (hydroxyl) stretching assigned to the hydroxyl group from glucose. Other peaks at 1550, 1450, 1388, 1296, 1071, 841, and 606 correspond to the stretching vibration of N-O from a nitro compound, C-H bending from an alkane, C-N bending vibration of amine, C-N stretching from aromatic amine, C-O stretching vibration of alcohol, C=C bending of alkene and C-Cl from halo compounds. The result is similar to an already published report on the FTIR of pure crystalline AgNPs [24,74]. The functional group of NO_3^- is from the starting material, which is $AgNO_3$. [49,80]. The Ag-O vibrational peak was observed around 410 cm$^{-1.}$ All are the functional group covering AgNPs.

3.3. *Adsorption of bacterial DNA*

It is well-known that the adsorption of DNA onto synthesized nanoparticles in solution depends on factors such as the nature, size, charge, binding characteristic of the nanoparticles, and the buffering condition [66]. These factors are essential in solution chemistry and solid-phase extraction of certain metals like nanomaterials and polymeric species. Besides, adding acid and base solution to adjust the pH of a working solution plays a vital role in sorption processes, especially in adsorption capacity [29].

3.3.1. *Effects of varying pH of DNA solution*

The effect of varying pH (pH 2 to 9) on the DNA adsorption onto as-synthesized samples represented as BD1, BD2, and BD3 was carried out at an initial DNA concentration of 9.92 μg/mL, adsorbent dose of 20 mg, equilibrium time of 360 mins and at room temperature. We observed that bacterial DNA could adsorb on the as-synthesized samples of AgNPs (BD1, BD2, and BD3) at a wide pH range. DNA percentage removal (%R) increases significantly from basic to acidic pH (50.26 - 87.61 %, 65.80 - 87.79 %, and 69.23 - 87.92%) for BD1 BD2 BD3, respectively, and the result is shown in Fig. 8. This result is similar to data obtained on the adsorption of ARGs embedded in DNA onto graphene oxide nanosheets [91]. The removal efficiency can increase to 99% when the initial pH is strongly acidic (initial pH 1.0) and if there is a competing ion in the solution and surface modification of adsorbents. The adsorption of bacterial DNA onto the as-synthesized samples depends on the adsorbent's surface charge, and the influence of pH solution since the adsorbate (DNA) has a high negative charge. From this study, removal efficiency from pH 2 to 6 was in the range (87.61-70.7%, 87.79-77.20%, 87.92-78.36% for BD1, BD2, and BD3, respectively) and exhibited high % removal efficiencies. It is because adsorbent surface charge acquires more positive charge particles from the acidic pH solution increasing the electrostatic attraction between

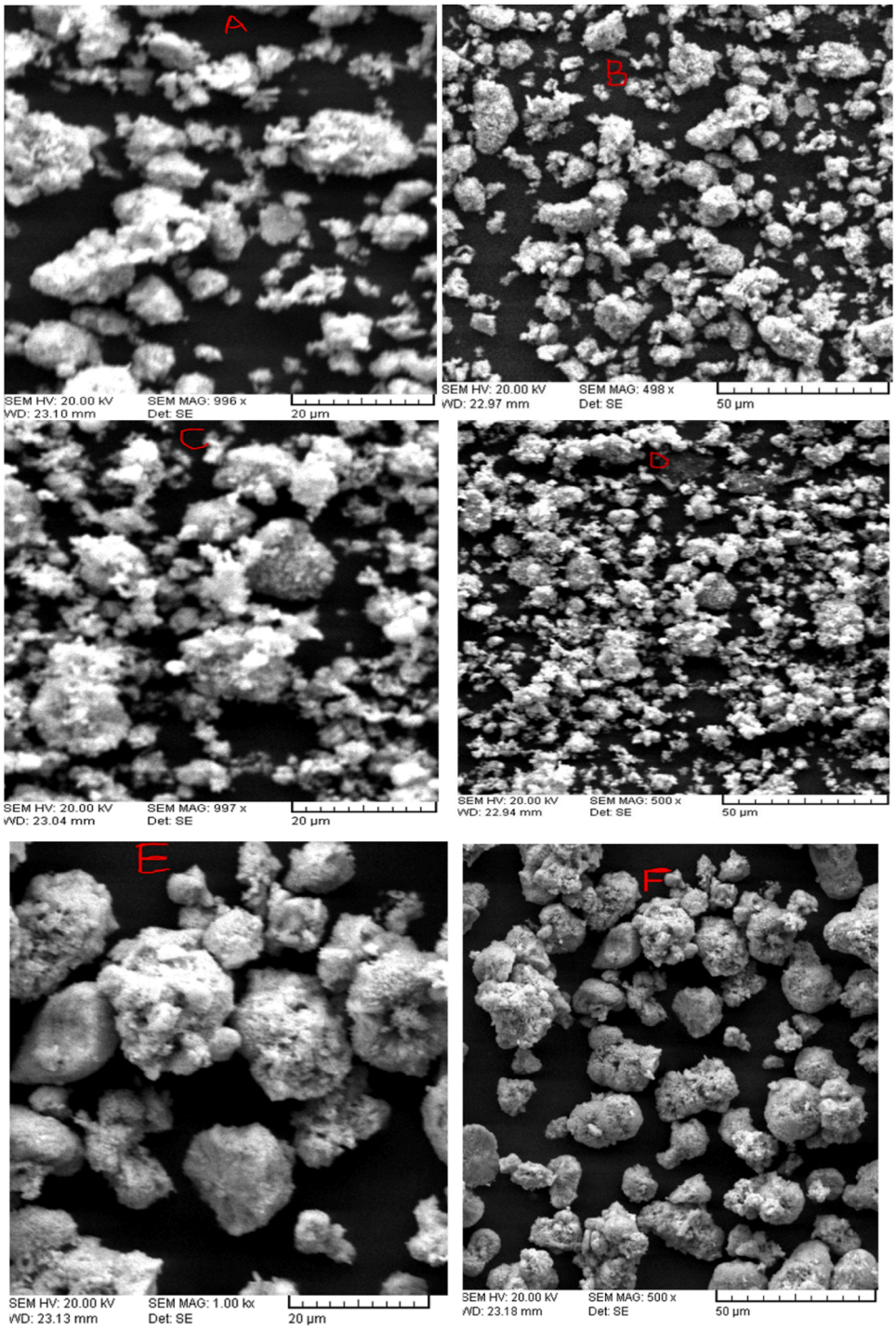

Fig. 3. A, B, C, D, E, and F: SEM images of BD1, BD2, and BD3 at low (A, C, E) and higher (B, D, F) magnifications showing spherical and irregular multi-branched morphology of the particles.

adsorbate charge species (negative) and adsorbent charged particles (positive), thereby leading to high removal efficiencies in all the adsorbents by electrostatic interaction [5,95]. Also, it can be attributed to changes in the surface charge of the adsorbents in an aqueous solution and dissociation of the functional group on the adsorptive site [84]. At pH 7 (neutral), the removal efficiency is 70 %, similar to the result obtained at neutral pH during the adsorption of DNA onto graphene oxide under Fluorescently Labeled Oligonucleotide [91]. The removal efficiencies of pH 8-9 decreased to 55.8-50.26 %, 67.42-65.80 %, and 69.84-69.23 % for BD1, BD2 and

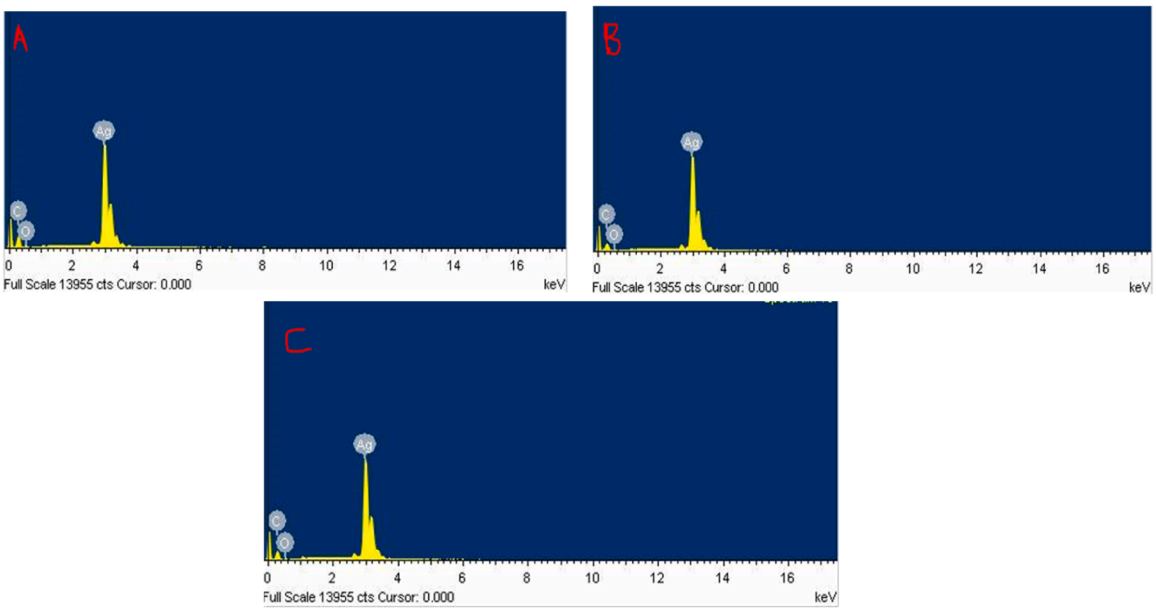

Fig. 4. A, B, C: Energy-dispersive X-ray spectroscopy (EDX) of AgNPs represented as BD1 (0.1 M), BD2 (0.5 M), BD3 (1.0 M) showing the elemental composition of the nanoparticles.

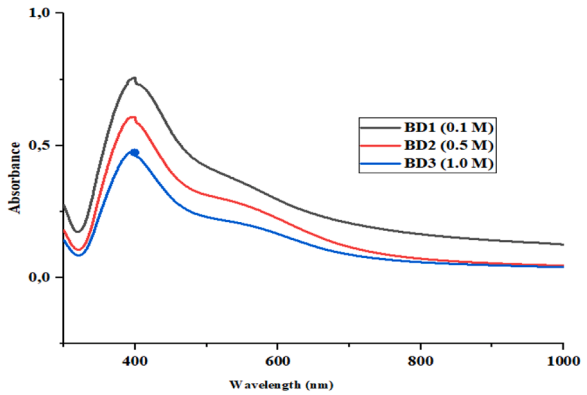

Fig. 5. UV-visible absorption spectra of different molar concentrations of the as-synthesized AgNPs.

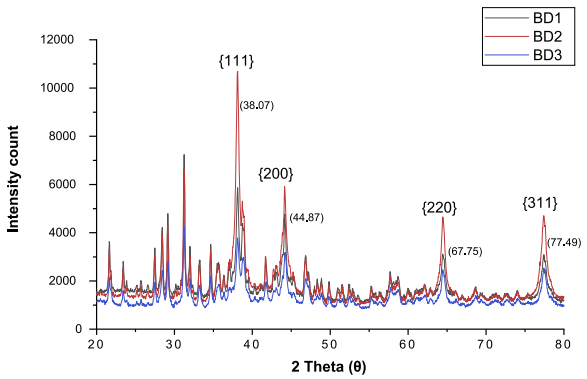

Fig. 6. XRD pattern for the as-synthesized AgNPs of different molar concentrations represented as BD1 (0.1 M), BD2 (0.5 M), and BD3 (1.0 M).

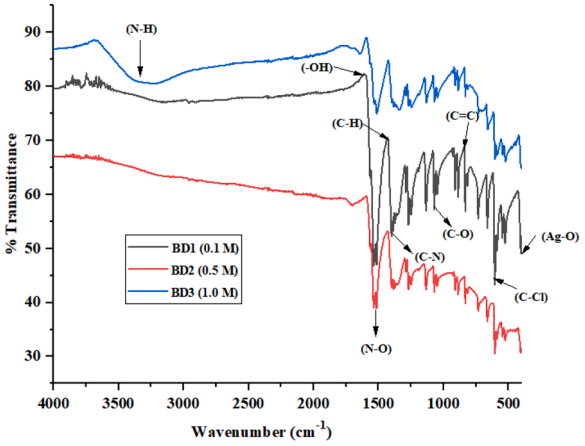

Fig. 7. FTIR spectra of the as-synthesized AgNPs represented as BD1, BD2, and BD3.

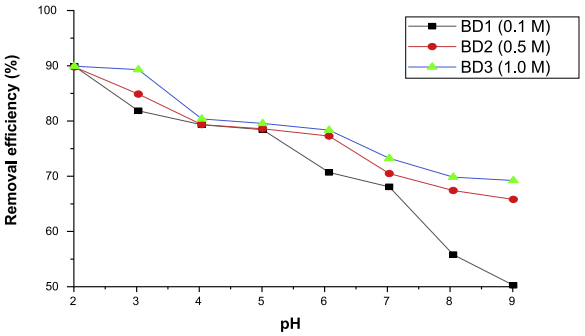

Fig. 8. Effects of pH for removal of bacteria DNA harboring ARGs with as-synthesized samples of AgNPs (Concentration = 9.92 μg/mL; adsorbents dose = 20 mg, reaction time = 360 mins and at room temperature).

BD2 respectively. It is due to charge repulsion in the adsorptive site [45]. The DNA adsorption onto as-synthesized AgNPs samples is more favorable under acidic conditions than the neutral or alkaline conditions due to excess H^+ ions, increasing the positive charge in the adsorbents.

Interestingly, the final pH increases slightly from pH 2-6 (acidic condition) but decreases from pH 8-9 (alkaline condition), except for the initial pH of 6.9, whose final pH is 5.41, 5.61, and 5.60 for BD1, BD2, and BD3 (Table 1a, b, c). These slight increases and decreases in the final pH may be attributed to the addition of hydrogen (H^+) and hydroxide ($O.H.^-$) ions released into the solution, leading to depurination and hydrolysis of the phosphate group and a nitrogenous base [9]. For the stability of the working DNA, pH 7 (neutral) was chosen for further experiments. Because, at pH 2-6 and 8-9, the depurination of DNA may gradually occur, leading to DNA damage. But at neutral pH, all the four DNA bases (pH 7.0) are charged-neutral, and each phosphate group carries a negative charge ($pK_a < 2$).

3.3.2. Effects of contact time and initial DNA concentrations

The effects of contact time on the adsorption capacity of DNA onto the samples of as-synthesized AgNPs at different initial DNA concentrations (4.98, 9.92, and 14.98 μg/mL) are shown in Fig. 9. The experiment was conducted at room temperature, with a fixed adsorbent dose of 20 mg and neutral pH. The data obtained for BD1, BD2, and BD3 at an initial DNA concentration of 4.98, 9.92, and 14.98 μg/mL were instantaneous during the initial period and gradually slowed and stagnated with the increase in contact time. Based on the initial DNA concentrations of 4.98, 9.92, and 14.98 μg/mL, the optimum DNA removal duration was 180, 195, and 225 mins for BD1, BD2, and BD3, respectively. For the effects of initial DNA concentration, the adsorption capacities for BD2 and BD3 increased as the initial concentrations rose from 4.98 to 14.98 μg/mL but decreased in BD1.

Furthermore, an increase in the initial concentration of DNA increased the adsorption capacity for all three adsorbents. This report confirmed that most adsorptive sites are available at the initial stage and the vacant site facilitates DNA binding onto the adsorbent through electrostatic interaction forces [62]. It was also observed that equilibrium adsorption capacities on BD1, BD2, and BD3 at different initial DNA concentrations show an increasing trend because of the driving force provided by DNA concentration [55], electrostatic screening effects, and generation of intermolecular hydrogen bond [51]. These reports confirmed that the success of any adsorption process depends highly on the initial concentration of DNA. It was noticed that adsorption of DNA onto samples of BD1,

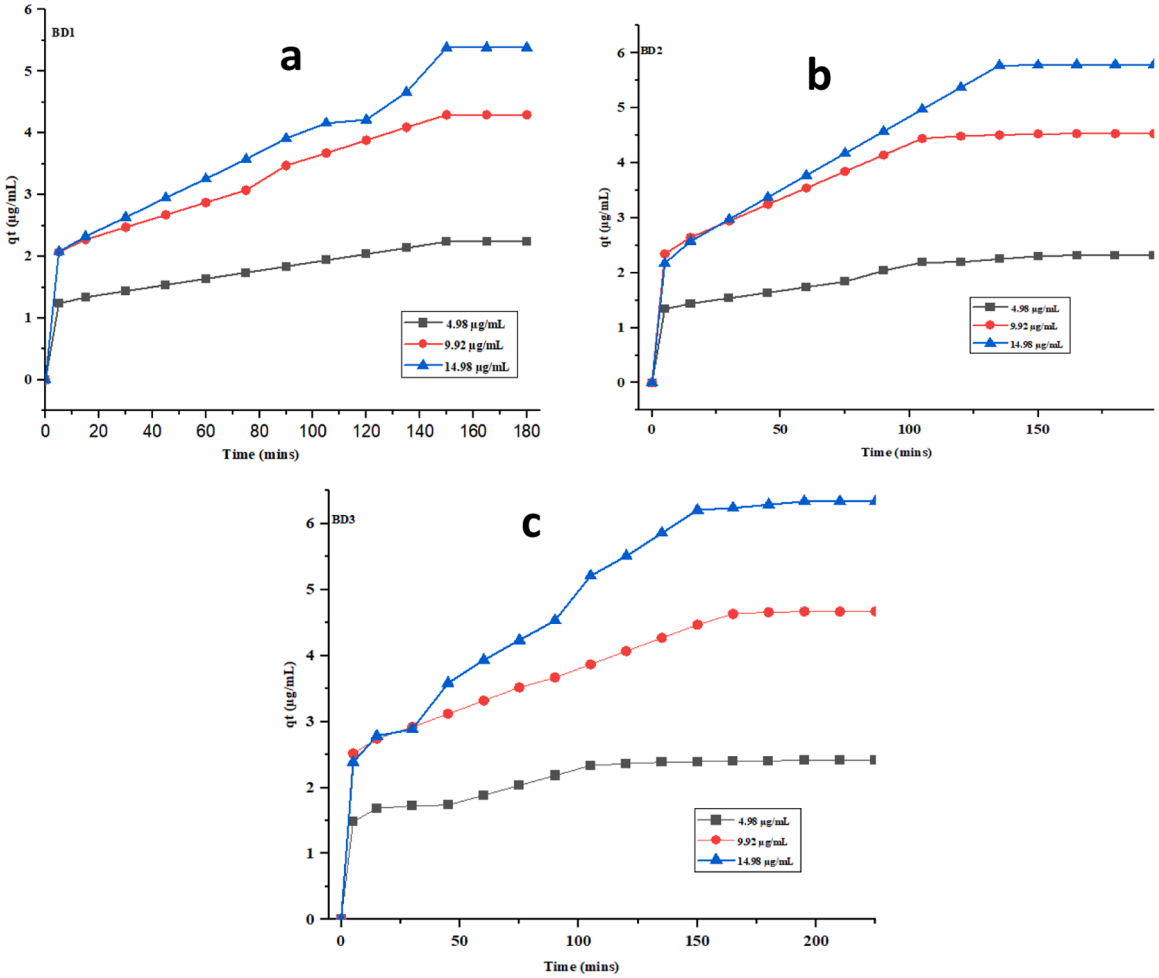

Fig. 9. a, b, c: Represents the effect of contact time for BD1, BD2 and BD3 respectively at different adsorbate (DNA) concentrations (4.98, 9.92 and 14.98 µg/mL); reaction time of 180, 195, and 225 mins, speed = 300 rpm, and pH = 6.9 at room temperature.

BD2, and BD3 reached equilibrium at different time intervals. It may be attributed to the different molar concentrations of the variables adopted during the synthesis of AgNPs. Also, the equilibrium time is dependent on the DNA solution's initial concentration. Fixed adsorbate initial concentration of 9.92 µg/mL and contact time of 180, 195, and 225 mins for BD1, BD2, and BD3 respectively were maintained for the subsequent adsorption experiments.

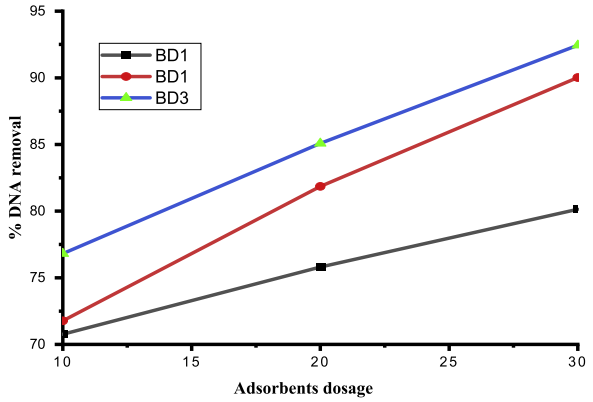

Fig. 10. Effect of adsorbent dose on the removal of DNA, adsorbate concentration = 9.92 µg/mL, reaction time = 225 mins; Speed = 300 rpm, pH = 6.9, and at room temperature.

3.3.3. Effects of adsorbents dosage

The adsorbent dosage in working solutions plays a vital role in DNA uptake and the percentage removal efficiency of DNA. It is one of the best parameters for determining the optimum condition for the adsorption process. It influenced adsorption through adsorbent material capacity [18,78]. In this study, the adsorption of DNA onto BD1, BD2, and BD3 were investigated by varying the adsorbent quantity from 10 mg to 30 mg in solutions while maintaining a fixed DNA working concentration of 9.92 μg/mL, pH of 6.9, contact time of 180, 195, and 225 mins for BD1, BD2, and BD3 respectively, speed of 300 rpm at room temperature. Fig. 10 shows the percentage (%) adsorption efficiency plot against adsorbent concentration (mg) of BD1, BD2, and BD3. Adsorption efficiency increases with adsorbent concentration [66]. Thus, the initial concentration of DNA decreased with an increase in the adsorbent dose from 10 to 30 mg. The % removal efficiencies increases from 70.76 to 80.14%, 71.77 to 90.02%, and 76.81 to 92.43% for BD1, BD2, BD3 respectively. This result may be attributed to two reasons: (1) the amount of adsorption efficiency per unit mass depends on the concentration gradient between adsorbate and the increase in adsorbent concentration [6,92]. (2) the abundance of the active sites on the adsorbent for adsorbate sorption increases as the adsorbent dose increases [1]. This result agrees with published reports on the effects of adsorbent dose on the adsorption process [64,81]. It suggests that a high adsorbent dose increases the adsorptive sites, increasing attraction between DNA molecules and AgNPs [50]. Therefore, the optimum dosage for DNA adsorption onto BD1, BD2, and BD3 is 30 mg, and economical dosage for removing DNA from water.

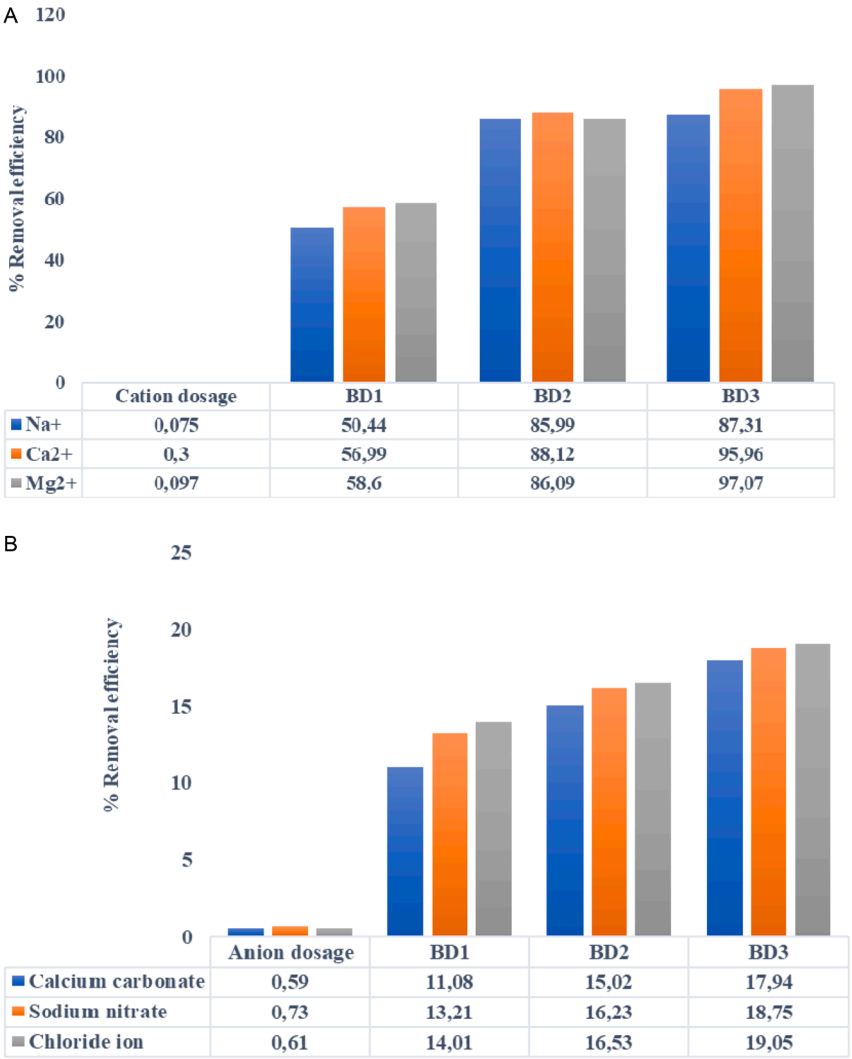

Cation dosage	BD1	BD2	BD3
Na+	0,075	50,44	85,99	87,31
Ca2+	0,3	56,99	88,12	95,96
Mg2+	0,097	58,6	86,09	97,07

Anion dosage	BD1	BD2	BD3
Calcium carbonate	0,59	11,08	15,02	17,94
Sodium nitrate	0,73	13,21	16,23	18,75
Chloride ion	0,61	14,01	16,53	19,05

Fig. 11. (a) Effects of competing ions (cations) on DNA adsorption onto BD1, BD2 and BD3 (pH = 6.9, adsorbent dose = 30 mg, DNA working concentration = 9.92 μg/mL, Contact time =BD1(180 mins), BD2 (195 mins) and, BD3 (225 mins) at room temperature. (b) Effects of competing ions (anions) on DNA adsorption onto BD1, BD2 and BD3 (pH = 6.9, adsorbent dose = 30 mg, DNA working concentration = 9.92 μg/mL, Contact time =BD1(180 mins), BD2 (195 mins) and, BD3 (225 mins) at room temperature.

3.3.4. Effects of competitive cations

Several background ions are detected in the wastewater treatment plants, which may interfere with the adsorbent's DNA uptake through competitive binding or complexation [38]. Batch equilibrium studies were investigated to ascertain the effect of cations (Na^+, Ca^{2+}, and Mg^{2+}) and anions (Cl^-, CO_3^{2-}, and NO_3^-) onto DNA uptake by adsorbents (BD1, BD2, and BD3). The solutions containing 0.075, 0.3, and 0.097 g (Na^+, Ca^{2+}, Mg^{2+}) for cations and 0.59, 0.73, and 0.61 g for anions (CO_3^{2-}, NO_3^-, and Cl^-) with fixed adsorbents dose of 30 mg, pH of 6.9, DNA working concentration of 9.92 μg/mL, contact time of 180, 195, and 225 mins for BD1, BD2, and BD3 at room temperature were agitated separately. The results are shown in Fig. 11. Fig. 11a demonstrated that DNA adsorption onto all the adsorbents was optimum for Mg^{2+} and Ca^{2+} with removal efficiencies of 89.23 to 91.39%, 93.89 and 95.0, 97.10, and 99.94 % for BD1, BD2, and BD3 compared to Na^+ (50.44, 56.99, and 58.66) in all the adsorbents. However, DNA adsorption efficiencies increase compared to the values obtained in the absences of cations, indicating competitive complexation with some other ions [66]. For the presence of anions shown in Fig. 11b, all the adsorbents' DNA removal efficiencies drastically decreased from 11.08 to 17.94, 13.21 to 18.75, and 14.01 to 19.05 % for BD1 BD2, and BD3, respectively. It was observed that the presence of CO_3^{2-}, NO_3^-, and Cl^- shows no significant effect on DNA adsorption.

This information is considerably helpful for the adsorption of DNA in natural water samples that contain a large amount of alkaline earth metal ions [86]. Thus, AgNPs have good adsorption efficiency and a high affinity for DNA in solution. Therefore, this study shows that different molar concentrations of as-synthesized AgNPs are potential adsorbents for DNA removal from an aqueous solution containing competing ions.

3.4. Adsorption model

Modeling the adsorption process is vital in removing targeted pollutants during water treatment. They predict or describe the comprehensive nature of adsorbate interaction with adsorbents, surface properties, and adsorption system design. In this study, mathematical equations of each model presented in table 1 were employed to improve the adsorption system design and ensure that different molar concentrations of synthesized AgNPs (BD1, BD2, and BD3) have good removal efficiency for bacteria DNA. Besides, they were used to establish the best reasonable correlation for equilibrium curves and characteristics. These models provided an insight into the adsorbent's surface properties, such as maximum adsorbent capacity over adsorbate and its affinity [15].

Tables 3a, 3b and 3c

3.4.1. Isotherm model

This study used isotherm equations from Freundlich and Langmuir models to describe the equilibrium characteristics of adsorbate-adsorbents interaction. They helped in determining the maximum adsorption capacity at equilibrium. Their basic assumption differs in the adsorption process. The Freundlich isotherm assumed that cation and anions are adsorbed on a heterogeneous surface (multilayer adsorption), forming an attractive surface force [40]. Whereas the Langmuir model assumes monolayer adsorption at a homogenous site within the adsorbent surface i.e., no further adsorption occurs once the DNA molecules occupy the adsorptive site [15]. The result of the isotherm study on DNA adsorption onto different molar concentrations of as-synthesized AgNPs and the isotherm parameters are summarized in Table 4. The Chi-square (X^2) was used to evaluate the experimental and calculated data difference. The model with a smaller X^2 indicated the best fit for the study [60].

$$X^2 = \sum \frac{(qe^{\exp} - qe^{cal})^2}{qe^{cal}} \tag{4a}$$

Among the two-isotherm models employed, experimental data of BD1 and BD2 were best described by the Langmuir model, with the highest coefficient parameter and a reduced Chi-square (X^2) ($R^2 = 0.97625$ and $X^2 = 0.12142$ for BD1) ($R^2 = 0.96049$ and $X^2 = 0.24403$ for BD2). For BD3, Langmuir is fairly fitted with $R^2 = 0.850108$ and reduced $X^2 = 1.00914$ compared to Freundlich model ($R^2 = 0.72646$ and reduced $X^2 = 1.85363$). The best fitting of the Langmuir model on BD1 and BD2 denoted that adsorption of bacteria DNA molecules occurred at specific homogenous sites within the adsorbent surfaces [29]. The maximum adsorption capacity (qmax), widely used to compare the efficiency of adsorbents, was obtained in Langmuir isotherm, and they are 0.06595 μg/mL, 0.0665 μg/mL, and 0.66094 μg/mL for BD1, BD2, and BD3.

The separator factor ($R_{L.}$) relating to the Langmuir isotherm was employed in the study. It was used to evaluate the feasibility of adsorption onto the adsorbent [29] using the Equation below:

$$RL = 1/1 + Ci \times KL \tag{5}$$

Ci (μg/mL) is the initial DNA concentration, and K.L. is the Langmuir constant. Note $R_{L.}$ indicates the adsorption status, and when $R_L = 0$, it is irreversible; when $0 < R_{L.} < 1$, it is favorable; when $R_{L.} = 1$, it is linear, and when $R_{L.} > 1$, it is unfavorable. From Langmuir's study, the range of $R_{L.}$ for BD1, BD2, and BD3 are 0.0706, 0.1958, and 0.0000365. This result confirmed that the adsorption of DNA

Table 3a
Represents the initial and final pH of BD1 before and after adsorption process.

pH	2	3	4	5	6	7	8	9
Initial pH	2.01	3.01	4.03	5.04	5.9	6.90	8.23	9.31
Final pH	2.89	3.50	4.91	5.21	5.41	5.83	5.91	6.30

Table 3b
Represents the initial and final pH of BD2 before and after adsorption process.

pH	2	3	4	5	6	7	8	9
Initial pH	2.01	3.03	4.24	5.32	5.91	6.85	8.11	9.21
Final pH	2.91	3.69	5.11	5.75	5.61	6.01	6.11	6.71

Table 3c
Represents the initial and final pH of BD3 before and after adsorption process.

pH	2	3	4	5	6	7	8	9
Initial pH	2.03	3.16	4.13	5.34	6.39	6.83	8.30	9.2
Final pH	2.88	3.70	5.41	5.41	5.63	5.72	6.18	6.87

Table 4
Representation of isotherm parameters for the bacteria DNA adsorption onto BD1, BD2 and BD3.

Isotherm	Parameter	BD1	BD2	BD3
Langmuir	qmax (μg/mL)	0.06595	0.06865	0.660939
	$K_{L.}$ (μg/g)	0.01179	0.82443	0.53278
	$R_{L.}$	0.07061	0.19586	0.0000365
	X^2	0.12142	0.24403	1.00914
	R^2	0.97625	0.96049	0.90108
Freundlich	K_f (μg/g)	3.38305	4.05012	4.83834
	n	2.89176	3.15705	4.49655
	X^2	0.51699	0.82316	1.85363
	R^2	0.89886	0.86674	0.72646

onto different as-synthesized AgNPs is favorable.

3.4.2. kinetic model

The adsorption kinetics is the utmost parameter considered during the adsorption process, and it determines the adsorption efficiency and rate of adsorbate uptake per contact time. To measure the adsorption equilibrium per contact time of different initial concentrations, the experimental data obtained in this study were fitted into two kinetic models, such as Natarajan and Khalaf first order and Pseudo-second-order kinetics (Table 2). The result shows that Pseudo second-order (PSO) kinetic is the best fit with the highest correlation value ranging from $R^2 = 0.90727$ to 0.98797 compared to First-order ($R^2 = 0.88234$ to 0.9567). The plot of t/qt versus t is a straight line, as shown in Fig. 12.

The slope and intercepts of the plots were obtained from the values of K_2 and qe, respectively. From the plots, the adsorption of bacteria DNA onto these adsorbents rose rapidly at the beginning and gradually slowed down over time. The adequate contact time was determined, and it is the time taken by these adsorbents (BD1, BD2, and BD3) to achieve between 70-90% DNA removal at equilibrium. From Fig. 12, the adequate contact time for DNA adsorption onto BD1, BD2, and BD3 were 140 mins, 150 mins, and 200 mins, and the equilibrium was achieved at 180 mins, 195 mins, and 225 mins, respectively. According to Pseudo-second-order kinetic, which was confirmed as the best fit for this study, the initial sorption rate or rate of adsorption (h) can be determined by using Eq. (6) [23]:

$$h = K2 \times qe2 \tag{6}$$

The value of h obtained from different initial concentrations using the three adsorbents increases in the same other as K_2. This indicates that a high adsorption rate occurs when the initial DNA concentration increases. The experimental value (qe^{exp}) and the calculated (qe^{cal}) of the three adsorbents in PSO show a good correlation with little consistency compared to First-order kinetic. We noticed that the pseudo-second-order constant (K_2) reduces with the increased initial concentration of adsorbate (DNA). It could be attributed to increased bacteria DNA concentration, reducing the diffusion of DNA molecules from the adsorptive site. The high correlation coefficient ranging from $R^2 = 0.90727$ to 0.98797 indicated that DNA adsorption by BD1, BD2, and BD3 was controlled by chemisorption [15]. It implies that during the adsorption process, the valency force exerted could be because of sharing or exchanging electrons between the synthesized AgNPs (BD1, BD2, and BD3) and the DNA molecule. The PSO kinetic parameters determined the equilibrium adsorption capacity, rate constant, initial sorption rate, and the percentage removal of DNA from these adsorbents. To compare the applicability and authenticity of each model fitted into the experimental data, the standard deviation (Δq) was calculated using Eq. (7) [57]:

$$\Delta q\ (\%) = 100 \times \sqrt{\frac{\sum[(qeexp - qecal)]}{\frac{qeexp}{n-1}}} \tag{7}$$

Other parameters such as correlation value (R^2), h, $K_{2,\ and}$ Δq, including the qe^{exp} and $qe^{cal,}$ are summarized in Table 5.

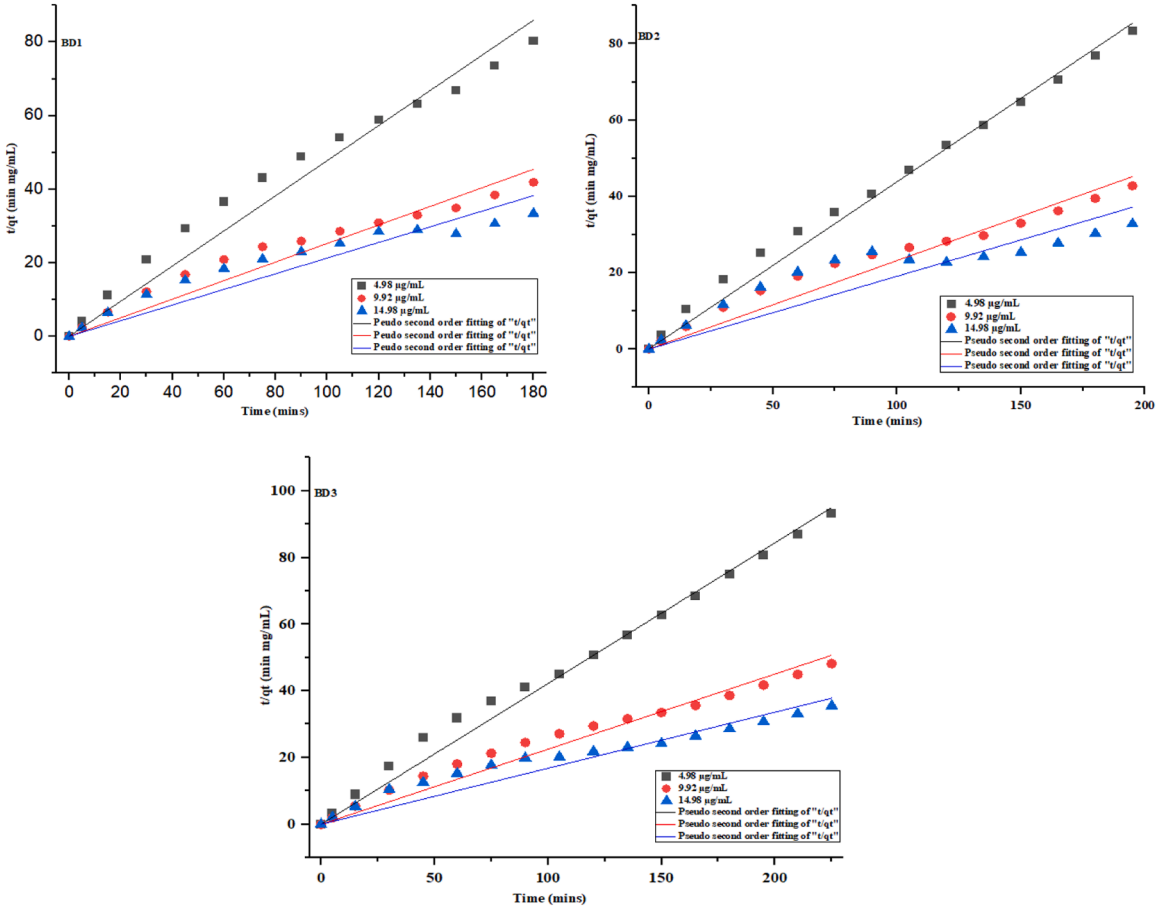

Fig. 12. Pseudo-Second-Order Kinetic plots for the adsorption of bacteria DNA onto BD1, BD2, and BD3 at different initial adsorbate concentrations (4.98, 9.92, and 14.98 µg/mL), pH = 6.9, and different time interval (180 mins, 195 mins and 225 mins for BD1, BD2, and BD3).

Table 5
Kinetic model parameters for bacteria DNA adsorption onto different molar concentrations of as-synthesized AgNPs represented as BD1, BD2, and BD3.

Kinetic models and Parameters	Adsorbent	C_i (µg/mL)	qe^{exp} (µg/g)	qe^{cal} (µg/g)	Δq (%)	K_1 ($mins^{-1}$)	h (µg/g)	R^2
Natarajan and Khalaf First order equation		4.98	2.24	3.80	49.24	4.23×10^{-5}	-	0.88234
	BD1	9.92	4.29	3.85	37.15	3.39×10^{-5}	-	0.91493
	BD2	14.98	4.21	2.29	32.25	3.31×10^{-5}	-	0.89862
	BD3	4.98	0.30	3.79	82.24	6.76×10^{-5}	-	0.95413
		9.92	0.81	6.38	21.87	2.56×10^{-5}	-	0.91465
		14.98	3.11	6.15	69.06	1.03×10^{-5}	-	0.92492
		4.98	0.15	2.32	102.2	3.98×10^{-5}	-	0.93133
		9.92	0.50	2.78	32.23	1.93×10^{-5}	-	0.91909
		14.98	2.30	3.29	30.49	2.56×10^{-5}	-	0.95670
Kinetic model parameters	**Adsorbent**	**C_i**	**qe^{exp} (µg/g)**	**qe^{cal} (µg/g)**	**Δq**	**K_2 ($mins^{-1}$)**	**h (µg/g)**	**R^2**
Pseudo-Second Order		4.98	2.24	2.16	2.52	1.10×10^{4}	5.25	0.95781
	BD1	9.92	4.29	4.25	2.08	0.46×10^{4}	8.77	0.92682
	BD2	14.98	4.21	4.19	1.06	0.41×10^{4}	7.78	0.90727
	BD3	4.98	0.30	0.29	2.34	0.65×10^{4}	0.06	0.98794
		9.92	0.81	0.76	4.37	0.46×10^{4}	0.28	0.94421
		14.98	3.11	2.98	2.94	0.41×10^{4}	3.71	0.90146
		4.98	0.15	0.18	14.14	0.64×10^{4}	0.02	0.98755
		9.92	0.50	0.49	1.41	0.46×10^{4}	0.11	0.96194
		14.98	2.30	2.27	2.91	0.39×10^{4}	2.01	0.90579

4. Conclusion

We concluded that the three different molar concentrations of AgNPs (BD1, BD2, and BD3) were subjected to the same operating parameters (pH, time, DNA concentrations, adsorbent dose, cation, and anions), and BD3 recorded the highest DNA removal efficiency.

CRediT authorship contribution statement

The authors declare that they have no known competing financial interests or personal relationships that could have appeared to influence the work reported in this paper.

Acknowledgments

The authors thank the South Africa Medical Research Council for financial support.

References

[1] N. Aarab, A. Hsini, A. Essekri, M. Laabd, R. Lakhmiri, A. Albourine, Removal of an emerging pharmaceutical pollutant (metronidazole) using PPY-PANi copolymer: Kinetics, equilibrium, and DFT identification of adsorption mechanism, Ground. Sustain. Dev. 11 (2020), https://doi.org/10.1016/j.gsd.2020.100416.
[2] K. Abe, N. Nomura, S. Suzuki, Biofilms: Hot spots of horizontal gene transfer (HGT) in aquatic environments, focusing on a new HGT mechanism, FEMS Microbiol. Ecol. 96 (2021) 1–12, https://doi.org/10.1093/FEMSEC/FIAA031.
[3] N. Agasti, N.K. Kaushik, One-Pot Synthesis of Crystalline Silver Nanoparticles, Am. J. Nanomater. 2 (2014) 4–7, https://doi.org/10.12691/ajn-2-1-2.
[4] S.F. Ahmed, M. Mofijur, S. Nuzhat, A.T. Chowdhury, N. Rafa, M.A. Uddin, A. Inayat, T.M.I. Mahlia, H.C. Ong, W.Y. Chia, P.L. Show, Recent developments in physical, biological, chemical, and hybrid treatment techniques for removing emerging contaminants from wastewater, J. Hazard. Mater. 416 (2021), https://doi.org/10.1016/j.jhazmat.2021.125912.
[5] M. Akter, M.T. Sikder, M.M. Rahman, A.K.M.A. Ullah, K.F.B. Hossain, S. Banik, T. Hosokawa, T. Saito, M. Kurasaki, A systematic review on silver nanoparticles-induced cytotoxicity: Physicochemical properties and perspectives, J. Adv. Res. 9 (2018) 1–16, https://doi.org/10.1016/j.jare.2017.10.008.
[6] A. Al Bsoul, M. Hailat, A. Abdelhay, M. Tawalbeh, A. Al-Othman, I.N. Al-kharabsheh, A.A. Al-Taani, Efficient removal of phenol compounds from water environment using Ziziphus leaves adsorbent, Sci. Total Environ. 761 (2021), https://doi.org/10.1016/j.scitotenv.2020.143229.
[7] A. Ali, M. Sattar, F. Hussain, M.H.K. Tareen, J. Militky, M.T. Noman, Single-step green synthesis of a highly concentrated and stable colloidal dispersion of core-shell silver nanoparticles and their antimicrobial and ultra-high catalytic properties, Nanomaterials 11 (2021), https://doi.org/10.3390/nano11041007.
[8] E. Alzahrani, Colorimetric Detection of Ammonia Using Synthesized Silver Nanoparticles from Durian Fruit Shell, J. Chem. (2020) 2020, https://doi.org/10.1155/2020/4712130.
[9] R. An, Y. Jia, B. Wan, Y. Zhang, P. Dong, J. Li, X. Liang, Non-enzymatic depurination of nucleic acids: Factors and mechanisms, PLoS One 9 (2014) 0–10, https://doi.org/10.1371/journal.pone.0115950.
[10] E. Aubertheau, T. Stalder, L. Mondamert, M.C. Ploy, C. Dagot, J. Labanowski, Impact of wastewater treatment plant discharge on the contamination of river biofilms by pharmaceuticals and antibiotic resistance, Sci. Total Environ. 579 (2017) 1387–1398, https://doi.org/10.1016/j.scitotenv.2016.11.136.
[11] F. Baranchesh, M. Munir, Strategies to combat antibiotic resistance in wastewater treatment plants, Front. Microbiol. 8 (2018), https://doi.org/10.3389/fmicb.2017.02603.
[12] Z. Bytesnikova, L. Richtera, K. Smerkova, V. Adam, Graphene oxide as a tool for antibiotic-resistant gene removal: a review, Environ. Sci. Pollut. Res. 26 (2019) 20148–20163, https://doi.org/10.1007/s11356-019-05283-y.
[13] Y. Che, Y. Yang, X. Xu, K. Brinda, M.F. Polz, W.P. Hanage, T. Zhang, Conjugative plasmids interact with insertion sequences to shape the horizontal transfer of antimicrobial resistance genes, Proc. Natl. Acad. Sci. U. S. A. 118 (2021), https://doi.org/10.1073/pnas.2008731118.
[14] A. Checcucci, P. Trevisi, D. Luise, M. Modesto, S. Blasioli, I. Braschi, P. Mattarelli, I am exploring the Animal Waste Resistome: The Spread of Antimicrobial Resistance Genes Through the Use of Livestock Manure, Front. Microbiol. 11 (2020) 1–9, https://doi.org/10.3389/fmicb.2020.01416.
[15] S. Chen, J. Zhang, C. Zhang, Q. Yue, Y. Li, C. Li, Equilibrium and kinetic studies of methyl orange and methyl violet adsorption on activated carbon derived from, Phragmites australis 252 (2010) 149–156, https://doi.org/10.1016/j.desal.2009.10.010.
[16] X. Chen, H. Yin, G. Li, W. Wang, P.K. Wong, H. Zhao, T. An, Antibiotic-resistance gene transfer in antibiotic-resistance bacteria under different light irradiation: Implications from oxidative stress and gene expression, Water Res 149 (2019) 282–291, https://doi.org/10.1016/j.watres.2018.11.019.
[17] F.A. Dawodu, C.U. Onuh, K.G. Akpomie, E.I. Unuabonah, Synthesis of silver nanoparticles from Vigna unguiculata stems as adsorbent for the malachite green in a batch system, S.N. Appl. Sci. 1 (2019), https://doi.org/10.1007/s42452-019-0353-3.
[18] H. Deng, J. Lu, G. Li, G. Zhang, X. Wang, Adsorption of methylene blue on adsorbent materials produced from the cotton stalk, Chem. Eng. J. 172 (2011) 326–334, https://doi.org/10.1016/j.cej.2011.06.013.
[19] P.A. Dhakras, Nanotechnology applications in water purification and wastewater treatment: A review, in: Proc. Int. Conf. Nanosci. Eng. Technol. ICONSET 2011, 2011, pp. 285–291, https://doi.org/10.1109/ICONSET.2011.6167965.
[20] T. Dimitriu, C. Lotton, J. Beńard-Capelle, D. Misevic, S.P. Brown, A.B. Lindner, F. Taddei, Genetic information transfer promotes cooperation in bacteria, Proc. Natl. Acad. Sci. U. S. A. 111 (2014) 11103–11108, https://doi.org/10.1073/pnas.1406840111.
[21] J. Dong, Y. Tang, A. Nzihou, Y. Chi, E. Weiss-hortala, M. Ni, Z. Zhou, Removal of antibiotic residues, antibiotic-resistant bacteria, and antibiotic resistance genes in municipal wastewater by membrane bioreactor systems, Water Res (2018), https://doi.org/10.1016/j.watres.2018.08.060.This.
[22] J.N. Edokpayi, A.M. Enitan-Folami, A.O. Adeeyo, O.S. Durowoju, A.O. Jegede, J.O. Odiyo, Recent trends and national water provision and wastewater treatment policies in South Africa, Water Conserv. Wastewater Treat. BRICS Nations (2020) 187–211, https://doi.org/10.1016/b978-0-12-818339-7.00009-6.
[23] S. Ekinci, Z. İlter, S. Ercan, E. Çınar, R. Çakmak, Magnetite nanoparticles grafted with murexide-terminated polyamidoamine dendrimers to remove lead (II) from aqueous solution: synthesis, characterization, adsorption, and antimicrobial activity studies, Heliyon 7 (2021), https://doi.org/10.1016/j.heliyon.2021.e06600.
[24] A.A. El-Kheshen, S.F.G. El-Rab, Effect of reducing and protecting agents on silver nanoparticles' size and antibacterial activity, Der Pharma Chem 4 (2012) 53–65.
[25] A.S. Ezeuko, M.O. Ojemaye, O.O. Okoh, A.I. Okoh, Journal of Water Process Engineering Potentials of metallic nanoparticles for removing antibiotic-resistant bacteria and antibiotic resistance genes from wastewater : A critical review, J. Water Process Eng. 41 (2021), 102041, https://doi.org/10.1016/j.jwpe.2021.102041.
[26] A. Fiorentino, A. Di Cesare, E.M. Eckert, L. Rizzo, D. Fontaneto, Y. Yang, G. Corno, Impact of industrial wastewater on the dynamics of antibiotic resistance genes in a full-scale urban wastewater treatment plant, Sci. Total Environ. (2019), https://doi.org/10.1016/j.scitotenv.2018.07.370.
[27] M. Foroughi, M. Khiadani, S. Kakhki, V. Kholghi, K. Naderi, S. Yektay, A systematic review of the effect of ozonation-based disinfection methods on the removal of antibiotic-resistant bacteria and resistance genes (ARB/ARGs) in water and wastewater treatment, Sci. Total Environ. 811 (2022), https://doi.org/10.1016/j.scitotenv.2021.151404.

[28] M. Foroughi, M. Khiadani, S. Kakhki, V. Kholghi, K. Naderi, S. Yektay, A systematic review of the effect of ozonation-based disinfection methods on the removal of antibiotic-resistant bacteria and resistance genes (ARB/ARGs) in water and wastewater treatment, Sci. Total Environ. (2022), https://doi.org/10.1016/j.scitotenv.2021.151404.

[29] J. Fu, Z. Chen, M. Wang, S. Liu, Jinghui Zhang, Jianan Zhang, R. Han, Q. Xu, Adsorption of methylene blue by a high-efficiency adsorbent (polydopamine microspheres): Kinetics, isotherm, thermodynamics, and mechanism analysis, Chem. Eng. J. 259 (2015) 53–61, https://doi.org/10.1016/j.cej.2014.07.101.

[30] J.A. Garrido-Cardenas, B. Esteban-García, A. Agüera, J.A. Sánchez-Pérez, F. Manzano-Agugliaro, Wastewater treatment by advanced oxidation process and their worldwide research trends, Int. J. Environ. Res. Public Health 17 (2020), https://doi.org/10.3390/ijerph17010170.

[31] P.J. Gomes, A.M. Ferraria, A.M. Botelho Do Rego, S.V. Hoffmann, P.A. Ribeiro, M. Raposo, Energy thresholds of DNA damage induced by U.V. radiation: An XPS study, J. Phys. Chem. B 119 (2015) 5404–5411, https://doi.org/10.1021/acs.jpcb.5b01439.

[32] A. Gray, The use of non-target high-resolution mass spectrometry screening to detect the presence of antibiotic residues in urban streams of Greensboro North Carolina, J. Environ. Heal. Sci. Eng. (2021), https://doi.org/10.1007/s40201-021-00688-9.

[33] Y. Guo, D. Li, S. Zheng, N. Xu, W. Deng, Utilizing Ag–Au core-satellite structures for colorimetric and surface-enhanced Raman scattering dual-sensing of Cu (II), Biosens. Bioelectron. 159 (2020), https://doi.org/10.1016/j.bios.2020.112192.

[34] M.G. Guzmán, J. Dille, S. Godet, Synthesis of silver nanoparticles by chemical reduction method and their antibacterial activity, Int. J. Chem. Biomol. Eng. 2 (2009) 104–111.

[35] R.A. Hamouda, M.H. Hussein, R.A. Abo-elmagd, S.S. Bawazir, Synthesis and biological characterization of silver nanoparticles derived from the cyanobacterium Oscillatoria limnetica, Nat. Res. (2019) 1–17.

[36] J.E. Han, L.L. Mohney, K.F.J. Tang, C.R. Pantoja, D.V. Lightner, Plasmid-mediated tetracycline resistance of Vibrio parahaemolyticus associated with acute hepatopancreatic necrosis disease (AHPND) in shrimps, Aquac. Reports. (2015), https://doi.org/10.1016/j.aqrep.2015.04.003.

[37] A.S. Hassanien, U.T. Khatoon, Synthesis and characterization of stable silver nanoparticles, Ag-NPs: Discussion on the applications of Ag-NPs as antimicrobial agents, Phys. B Condens. Matter 554 (2019) 21–30, https://doi.org/10.1016/j.physb.2018.11.004.

[38] L.S. Håvarstein, Bacterial gene transfer by natural genetic transformation, APMIS, Suppl 106 (1998) 43–46, https://doi.org/10.1111/j.1600-0463.1998.tb05647.x.

[39] H. He, P. Zhou, K.K. Shimabuku, X. Fang, S. Li, Y. Lee, M.C. Dodd, Degradation and Deactivation of Bacterial Antibiotic Resistance Genes during Exposure to Free Chlorine, Monochloramine, Chlorine Dioxide, Ozone, Ultraviolet Light, and Hydroxyl Radical, Environ. Sci. Technol. 53 (2019) 2013–2026, https://doi.org/10.1021/acs.est.8b04393.

[40] W. Huang, Y. Hu, Y. Li, Y. Zhou, D. Niu, Z. Lei, Z. Zhang, Citric acid-crosslinked β-cyclodextrin for simultaneous removal of bisphenol A, methylene blue, and copper: The roles of cavity and surface functional groups, J. Taiwan Inst. Chem. Eng. 82 (2018) 189–197, https://doi.org/10.1016/j.jtice.2017.11.021.

[41] S. Idris, Y.A. Iyaka, M.M. Ndamitso, E.B. Mohammed, M.T. Umar, Evaluation of Kinetic Models of Copper and Lead Uptake from Dye Wastewater by Activated Pride of Barbados Shell, Am. J. Chem. 1 (2012) 47–51, https://doi.org/10.5923/j.chemistry.20110102.10.

[42] C.D. Iwu, L. Korsten, A.I. Okoh, The incidence of antibiotic resistance within and beyond the agricultural ecosystem: A concern for public health, Microbiologyopen 9 (2020) 1–28, https://doi.org/10.1002/mbo3.1035.

[43] H.M. Jang, Y.B. Kim, S. Choi, Y. Lee, S.G. Shin, T. Unno, Y.M. Kim, Prevalence of antibiotic resistance genes from the effluent of coastal aquaculture, Environ. Pollut. (2018), https://doi.org/10.1016/j.envpol.2017.10.006.

[44] Murillo-Gelvez Jimmy, Dominic M.Di Toro, Herbert E. Allen, Richard F. Carbonaro, Reductive transformation of 3-Nitro-1,2,4-triazol-5-one (NTO) by Leonardite Humic Acid and Anthraquinone-2,6-disulfonate (AQDS), Environ. Sci. Technol. 55 (2021) 12973–12983.

[45] T.A. Jorge de Souza, L.R. Rosa Souza, L.P. Franchi, Silver nanoparticles: An integrated view of green synthesis methods, environmental transformation, and toxicity, Ecotoxicol. Environ. Saf. 171 (2019) 691–700, https://doi.org/10.1016/j.ecoenv.2018.12.095.

[46] Ş. Karadirek, H. Okkay, Ultrasound-assisted green synthesis of silver nanoparticle attached activated carbon for levofloxacin adsorption, J. Taiwan Inst. Chem. Eng. 105 (2019) 39–49, https://doi.org/10.1016/j.jtice.2019.10.007.

[47] A.H. Karim, A.A. Jalil, S. Triwahyono, S.M. Sidik, N.H.N. Kamarudin, R. Jusoh, N.W.C. Jusoh, B.H. Hameed, Amino modified mesostructured silica nanoparticles for efficient adsorption of methylene blue, J. Colloid Interface Sci. (2012), https://doi.org/10.1016/j.jcis.2012.07.043.

[48] A. Kumar, D. Pal, Antibiotic resistance and wastewater: Correlation, impact and critical human health challenges, J. Environ. Chem. Eng. 6 (2018) 52–58, https://doi.org/10.1016/j.jece.2017.11.059.

[49] R.R. Kumar, Mycogenic synthesis of silver nanoparticles by the Japanese environmental isolate Aspergillus tamari, Springer, 2012, https://doi.org/10.1007/s11051-012-0860-2.

[50] M.P. Kushalkar, B. Liu, J. Liu, Promoting DNA adsorption by acids and polyvalent cations: Beyond charge screening, Langmuir 36 (2020) 11183–11195, https://doi.org/10.1021/acs.langmuir.0c02122.

[51] X. Li, J. Zhang, H. Gu, Study on the adsorption mechanism of DNA with mesoporous silica nanoparticles in aqueous solution, Langmuir 28 (2012) 2827–2834, https://doi.org/10.1021/la204443j.

[52] K. Lv, S. Fichter, M. Gu, J. März, M. Schmidt, An updated status and trends in actinide metal-organic frameworks (An-MOFs): From synthesis to application, Coord. Chem. Rev. 446 (2021), 214011, https://doi.org/10.1016/j.ccr.2021.214011.

[53] M.M. Mcconnell, L. Truelstrup, R.C. Jamieson, K.D. Neudorf, C.K. Yost, A. Tong, Science of the Total Environment Removal of antibiotic resistance genes in two tertiary level municipal wastewater treatment, Plants 643 (2018) 292–300.

[54] G. Metreveli, A. Philippe, G.E. Schaumann, Disaggregation of silver nanoparticle homoaggregates in a river water matrix, Sci. Total Environ. 535 (2015) 35–44, https://doi.org/10.1016/j.scitotenv.2014.11.058.

[55] S.G. Michael, I. Michael-Kordatou, V.G. Beretsou, T. Jäger, C. Michael, T. Schwartz, D. Fatta-Kassinos, Solar photo-Fenton oxidation followed by adsorption on activated carbon for the minimization of antibiotic resistance determinants and toxicity present in urban wastewater, Appl. Catal. B Environ. 244 (2019) 871–880, https://doi.org/10.1016/j.apcatb.2018.12.030.

[56] Y. Miyah, A. Lahrichi, M. Idrissi, A. Khalil, F. Zerrouq, Adsorption of methylene blue dye from aqueous solutions onto walnut shell powder: Equilibrium and kinetic studies, Surfaces Interfaces (2018), https://doi.org/10.1016/j.surfin.2018.03.006.

[57] M.K. Miyittah, F.W. Tsyawo, K.K. Kumah, C.D. Stanley, J.E. Rechcigl, Suitability of Two Methods for Determination of Point of Zero Charge (PZC) of Adsorbents in Soils, Commun. Soil Sci. Plant Anal. 47 (2016) 101–111, https://doi.org/10.1080/00103624.2015.1108434.

[58] A. Monshi, M.R. Foroughi, M.R. Monshi, Modified Scherrer Equation to Estimate More Accurately Nano-Crystallite Size Using XRD, World J. Nano Sci. Eng. 2012 2012 (2012) 154–160.

[59] R.P. Nippes, P.D. Macruz, G.N. da Silva, M.H. Neves Olsen Scaliante, A critical review on the environmental presence of pharmaceutical drugs tested for the covid-19 treatment, Process Saf. Environ. Prot. (2021), https://doi.org/10.1016/j.psep.2021.06.040.

[60] O.A. Obijole, G.W. Mugera, R. Mudzielwana, P.G. Ndungu, A. Samie, A. Babatunde, Hydrothermally treated aluminosilicate clay (HTAC) for remediation of fluoride and pathogens from water: Adsorbent characterization and adsorption modeling, Water Resour. Ind. (2021), https://doi.org/10.1016/j.wri.2021.100144.

[61] K.M.M. Pärnänen, C. Narciso-Da-Rocha, D. Kneis, T.U. Berendonk, D. Cacace, T.T. Do, C. Elpers, D. Fatta-Kassinos, I. Henriques, T. Jaeger, A. Karkman, J. L. Martinez, S.G. Michael, I. Michael-Kordatou, K. O'Sullivan, S. Rodriguez-Mozaz, T. Schwartz, H. Sheng, H. Sørum, R.D. Stedtfeld, J.M. Tiedje, S.V. Della Giustina, F. Walsh, I. Vaz-Moreira, M. Virta, C.M. Manaia, Antibiotic resistance in European wastewater treatment plants mirrors the prevalence of clinical antibiotic resistance, Sci. Adv. 5 (2019), https://doi.org/10.1126/sciadv.aau9124.

[62] M.N. Patel, P.A. Dosi, B.S. Bhatt, Synthesis, characterization, antibacterial activity, and DNA interaction studies of drug-based mixed ligand copper(II) complexes with terpyridines, Med. Chem. Res. 21 (2012) 2723–2733, https://doi.org/10.1007/s00044-011-9799-6.

[63] M. Pazda, J. Kumirska, P. Stepnowski, E. Mulkiewicz, Antibiotic resistance genes identified in wastewater treatment plant systems – A review, Sci. Total Environ. (2019), https://doi.org/10.1016/j.scitotenv.2019.134023.

[64] M.E. Peralta, S.A. Jadhav, G. Magnacca, D. Scalarone, D.O. Mártire, M.E. Parolo, L. Carlos, Synthesis and in vitro testing of thermoresponsive polymer-grafted core-shell magnetic mesoporous silica nanoparticles for efficient controlled and targeted drug delivery, J. Colloid Interface Sci. 544 (2019) 198–205, https://doi.org/10.1016/j.jcis.2019.02.086.
[65] S.R. Prasad, S.B. Teli, J. Ghosh, N.R. Prasad, V.S. Shaikh, G.M. Nazeruddin, A.G. Al-Sehemi, I. Patel, Y.I. Shaikh, A Review on Bio-inspired Synthesis of Silver Nanoparticles: Their Antimicrobial Efficacy and Toxicity, Eng. Sci. 16 (2021) 90–128, https://doi.org/10.30919/es8d479.
[66] S. Radi, S. Tighadouini, M. Bacquet, S. Degoutin, Y. Garcia, New hybrid material based on a silica-immobilized conjugated β-ketoenol-bipyridine receptor and its excellent Cu(II) adsorption capacity, Anal. Methods 8 (2016) 6923–6931, https://doi.org/10.1039/c6ay01825d.
[67] I.D. Rafraf, I. Lekunberri, A. Sànchez-Melsió, M. Aouni, C.M. Borrego, J.L. Balcázar, The abundance of antibiotic resistance genes in five municipal wastewater treatment plants in the Monastir Governorate, Tunisia. Environ. Pollut. 219 (2016) 353–358, https://doi.org/10.1016/j.envpol.2016.10.062.
[68] R. Rashid, I. Shafiq, P. Akhter, M.J. Iqbal, M. Hussain, A state-of-the-art review on wastewater treatment techniques: the effectiveness of adsorption method, Environ. Sci. Pollut. Res. 28 (2021) 9050–9066, https://doi.org/10.1007/s11356-021-12395-x.
[69] M.A. Raza, Z. Kanwal, A. Rauf, A.N. Sabri, S. Riaz, Size- and Shape-Dependent Antibacterial Studies of Silver Nanoparticles Synthesized by Wet Chemical Routes, MDPI 6 (2016) 74, https://doi.org/10.3390/nano6040074.
[70] B. Reidy, A. Haase, A. Luch, K.A. Dawson, I. Lynch, Mechanisms of silver nanoparticle release, transformation, and toxicity: A critical review of current knowledge and recommendations for future studies and applications, Materials (Basel) 6 (2013) 2295–2350, https://doi.org/10.3390/ma6062295.
[71] L. Riaz, M. Anjum, Q. Yang, R. Safeer, A. Sikandar, H. Ullah, A. Shahab, W. Yuan, Q. Wang, Treatment technologies and management options of antibiotics and AMR/ARGs, Antibiotics and Antimicrobial Resistance Genes in the Environment, Elsevier Inc, 2020, https://doi.org/10.1016/b978-0-12-818882-8.00023-1.
[72] P.R. Rout, T.C. Zhang, P. Bhunia, R.Y. Surampalli, Treatment technologies for emerging contaminants in wastewater treatment plants: A review, Sci. Total Environ. 753 (2021), https://doi.org/10.1016/j.scitotenv.2020.141990.
[73] S. Salaheen, M. Peng, B. Debabrata, Replacement of Conventional Antimicrobials and Preservatives in Food Production to Improve Consumer Safety and Enhance Health Benefits. Microb, Food Saf. Preserv. Tech (2014) 324–347, https://doi.org/10.1201/b17465-20.
[74] M. Shahjahan, Synthesis and Characterization of Silver Nanoparticles by Sol-Gel Technique, Nanosci. Nanometrol. 3 (2017) 34, https://doi.org/10.11648/j.nsnm.20170301.16.
[75] S. Shaikh, N. Nazam, S.M.D. Rizvi, K. Ahmad, M.H. Baig, E.J. Lee, I. Choi, Mechanistic insights into the antimicrobial actions of metallic nanoparticles and their implications for multidrug resistance, Int. J. Mol. Sci. 20 (2019) 1–15, https://doi.org/10.3390/ijms20102468.
[76] V.K. Sharma, N. Johnson, L. Cizmas, T.J. McDonald, H. Kim, A review of the influence of treatment strategies on antibiotic-resistant bacteria and antibiotic resistance genes, Chemosphere (2016), https://doi.org/10.1016/j.chemosphere.2015.12.084.
[77] D. Shi, H. Hao, Z. Wei, D. Yang, J. Yin, H. Li, Z. Chen, Z. Yang, T. Chen, S. Zhou, H. Wu, J. Li, M. Jin, Combined exposure to non-antibiotic pharmaceutics and antibiotics in the gut synergistically promotes the development of multidrug resistance in Escherichia coli. Gut Microbes 14, J. Gut Microbes (2022), https://doi.org/10.1080/19490976.2021.2018901. Taylor and Francis.
[78] M.E. Sigrist, L. Brusa, H.R. Beldomenico, L. Dosso, O.M. Tsendra, M.B. González, C.L. Pieck, C.R. Vera, Influence of the iron content on the arsenic adsorption capacity of Fe/GAC adsorbents, J. Environ. Chem. Eng. 2 (2014) 927–934, https://doi.org/10.1016/j.jece.2014.02.013.
[79] Singh, S.P., Dubey, V., Mishra, A., Singh, Y., 2017. Silver nanoparticles: Biomedical applications, toxicity, and safety issues Silver nanoparticles: Biomedical applications, toxicity, and safety issues View project pharmacological investigation on analgesic and antipyretic potential of B-aescin View project.
[80] K.H. Sodha*, J.K. Jadav, H.P.G.A.K.J. Rathod, Characterization of silver nanoparticles synthesized by different chemical reduction methods, Int. J. Pharma Bio Sci. 2 (2015) 81–85.
[81] L.H. Tan, H. Xing, Y. Lu, DNA is a powerful tool for morphology control, spatial positioning, and dynamic assembly of nanoparticles, Acc. Chem. Res. 47 (2014) 1881–1890, https://doi.org/10.1021/ar500081k.
[82] Y. Titilawo, L. Obi, A. Okoh, Occurrence of virulence gene signatures associated with diarrhoeagenic and non-diarrhoeagenic pathovars of Escherichia coli isolates from some selected rivers in South-Western Nigeria, BMC Microbiol 15 (2015) 1–14, https://doi.org/10.1186/s12866-015-0540-3.
[83] F. Triggiano, C. Calia, G. Diella, M.T. Montagna, O. De Giglio, G. Caggiano, The role of urban wastewater in the environmental transmission of antimicrobial resistance: the current situation in Italy (2010–2019), Microorganisms 8 (2020) 1–12, https://doi.org/10.3390/microorganisms8101567.
[84] M.T. Uddin, M.A. Rahman, M. Rukanuzzaman, M.A. Islam, A potential low-cost adsorbent for the removal of cationic dyes from aqueous solutions, Appl. Water Sci. 7 (2017) 2831–2842, https://doi.org/10.1007/s13201-017-0542-4.
[85] E. Ugwoke, S.O. Aisida, A.A. Mirbahar, M. Arshad, I. Ahmad, T.kai Zhao, F.I. Ezema, Concentration-induced properties of silver nanoparticles and their antibacterial study, Surfaces and Interfaces (2020), https://doi.org/10.1016/j.surfin.2019.100419.
[86] P.E. Vandeventer, J.S. Lin, T.J. Zwang, A. Nadim, M.S. Johal, A. Niemz, Multiphasic DNA adsorption to silica surfaces under varying buffer, pH, and ionic strength conditions, J. Phys. Chem. B 116 (2012) 5661–5670, https://doi.org/10.1021/jp3017776.
[87] A.R. Vilchis-Nestor, J. Trujillo-Reyes, J.A. Colín-Molina, V. Sánchez-Mendieta, M. Avalos-Borja, Biogenic silver nanoparticles on carbonaceous material from sewage sludge for degradation of methylene blue in an aqueous solution, Int. J. Environ. Sci. Technol. 11 (2014) 977–986, https://doi.org/10.1007/s13762-013-0309-x.
[88] H. Wang, X. Qiao, J. Chen, X. Wang, S. Ding, Mechanisms of PVP in the preparation of silver nanoparticles, Mater. Chem. Phys. 94 (2005) 449–453, https://doi.org/10.1016/j.matchemphys.2005.05.005.
[89] Y. Yang, Y. Wang, Y. Peng, P. Cheng, F. Li, T. Liu, Acid-base buffering characteristics of non-calcareous soils: Correlation with physicochemical properties and surface complexation constants, Geoderma 360 (2020), 114005, https://doi.org/10.1016/j.geoderma.2019.114005.
[90] S. Yao, J. Ye, Q. Yang, Y. Hu, T. Zhang, L. Jiang, S. Munezero, K. Lin, C. Cui, Occurrence and removal of antibiotics, antibiotic resistance genes, and bacterial communities in hospital wastewater, Environ. Sci. Pollut. Res. 28 (2021) 57321–57333, https://doi.org/10.1007/s11356-021-14735-3.
[91] W. Yu, S. Zhan, Z. Shen, Q. Zhou, D. Yang, Graphene oxide nanosheet provides an efficient removal mechanism for antibiotic resistance genes from aquatic environments, Chem. Eng. J. 313 (2017) 836–846, https://doi.org/10.1016/j.cej.2016.10.107.
[92] A.S. Yusuff, L.T. Popoola, E.O. Babatunde, Adsorption of cadmium ion from aqueous solutions by the copper-based metal-organic framework: equilibrium modeling and kinetic studies, Appl. Water Sci. 9 (2019), https://doi.org/10.1007/s13201-019-0991-z.
[93] G. Zhang, W. Li, S. Chen, W. Zhou, J. Chen, Problems of conventional disinfection and new sterilization methods for antibiotic resistance control, Chemosphere 254 (2020), https://doi.org/10.1016/j.chemosphere.2020.126831.
[94] Zhang, X., Liu, Z., Shen, W., Gurunathan, S., 2016. Silver Nanoparticles : Synthesis, Characterization, Properties, Applications, and Therapeutic Approaches. https://doi.org/10.3390/ijms17091534.
[95] X. Zhang, M.R. Servos, J. Liu, Surface Science of DNA adsorption onto citrate-capped gold nanoparticles, Langmuir 28 (2012) 3896–3902, https://doi.org/10.1021/la205036p.